Contents lists available at ScienceDirect

Applied Materials Today

Engineering Ce/P-functionalized g-C$_3$N$_4$ for advanced ABS nanocomposites exhibiting unparalleled fire retardancy, enhanced thermal and mechanical properties

Guobo Huang [a,1,*], Siqi Huo [b,e,1], Jiahao Ren [a], Wei Chen [a], Haiqin Yang [a], Shenwei Xiao [a], Tianle Wang [a], Hong Peng [c], Pingan Song [b,d,**]

[a] School of Pharmaceutical and Chemical Engineering, Taizhou University, Taizhou 318000, China
[b] Centre for Future Materials, University of Southern Queensland, Springfield 4300, Australia
[c] School of Chemical Engineering, The University of Queensland, Brisbane, QLD 4072, Australia
[d] School of Agriculture and Environmental Science, University of Southern Queensland, Springfield 4300, Australia
[e] School of Engineering, University of Southern Queensland, Springfield 4300, Australia

ARTICLE INFO

ABSTRACT

The nanomaterials have been deeply explored as flame retardants for various polymeric materials due to their multifunctionality, but they often fail to significantly increase the limiting oxygen index (LOI) and vertical burning UL-94 rating, thus unable to meet industrial needs (LOI>27.0 % and UL-94 V-0 rating). Herein, we fabricated a cerium/phosphorus-doped g-C$_3$N$_4$ (Ce/P-CN) nanohybrid as a multifunctional high-efficiency fire retardant for acrylonitrile–butadiene–styrene (ABS). The Ce/P-CN nanoflakes featured a strengthening effect towards ABS, 10 wt% of which increased the tensile strength of ABS/(Ce/P-CN) by 33.8 %. Meanwhile, the ABS/(Ce/P-CN) nanocomposites showed remarkably enhanced high-temperature stability and carbonization performances relative to virgin ABS. Ce/P-CN simultaneously improved the anti-ignition, fire retardancy and smoke suppression of ABS due to the barrier effect of g-C$_3$N$_4$ nanoflakes and the catalytic carbonization effect of cerium and phosphorus. Notably, adding 10 wt% Ce/P-CN increased the LOI and UL-94 rating of ABS to 28.6 % and V-0, respectively, demonstrating its high flame-retardant efficiency. Thus, the high flame-retardant efficiency and multifunctionality enable Ce/P-CN to outperform previous flame retardants for ABS. This work offers a novel strategy for the development of high-efficiency g-C$_3$N$_4$ nanoflakes, which endow ABS with improved mechanical robustness and fire retardancy and show broad industrial prospects.

1. Introduction

Acrylonitrile–butadiene–styrene (ABS) resin is an important engineering thermoplastic for various industrial applications, *e.g.,* automobile parts, electric fans, and televisions, because of its low density, ease of processing, and good mechanical performances and chemical resistance [1–3]. The ABS resin is, however, easily ignited in the air and releases a large amount of heat and toxic smoke in the burning process, thus seriously endangering the environment and human safety [4,5]. Halogen-antimony synergistic system proved to be highly effective flame retardant for the ABS resin [6], but it was prohibited to use due to

its environmental pollution issues when burning [7].

To meet the policy requirements, many halogen-free flame retardants have been explored for the ABS resin [8–10]. Among various halogen-free alternatives, the nano flame retardants have stood out due to their good thermal stability, unique reinforcing effect and outstanding heat suppression [11–13]. For instance, Hong et al. [14] investigated the synergistic effect between metal hydroxide nanorods and graphene nanosheets (GNS) in ABS, and their results showed that the introduction of 2 wt% GNS and 4 wt% Co(OH)$_2$ endowed ABS nanocomposite with a 30.5 % reduction in peak heat release rate (PHRR). In addition, combining GNS and Co(OH)$_2$ effectively improved the mechanical

---

robustness of ABS nanocomposites, but led to the reduced toughness. Zhu et al. [15] developed boron dipyrromethene-modified MXene (BODIPY-MXene) nanosheets for flame retardant ABS. 0.5 wt% BODIPY-MXene can be homogeneously dispersed within ABS, and brough about a 27.8 % increase in tensile strength and a 24.5 % decrease in PHRR, demonstrating its multifunctionality. Generally, nano flame retardants are effective in suppressing the heat release of polymers at a low addition due to their nanostructures [16,17]. However, the nano flame retardants usually cannot impart high LOI and UL-94 rating to polymer nanocomposites, thereby failing to meet the industrial requirements, such as LOI>27.0 % and UL-94 V-0 rating [18,19]. The development of multifunctional nanoadditives, which not only effectively suppress the heat release during combustion, but also obviously increase LOI and UL-94 classification, has become a critical yet challenging direction of halogen-free flame retardants.

The two-dimensional (2D) nanomaterials, such as graphene, zirconium phosphate (ZrP), layered double hydroxides (LDHs), molybdenum (IV)sulfide (MoS_2), and graphitic carbon nitride (g-C_3N_4), feature high thermal stability and unique layered structure, therefore they are widely applied to flame retardant polymeric materials because of their outstanding physical barrier effect [20–24]. For example, Xu et al. [25] fabricated zinc hydroxystannate/β-Ni(OH)$_2$-modified g-C_3N_4 (g-C_3N_4/β-Ni(OH)$_2$/ZHS) nanosheets by a coprecipitation method. Their results presented that 3 wt% of g-C_3N_4/β-Ni(OH)$_2$/ZHS increased the LOI value of epoxy resin from 21.9 % to 26.2 %, and reduced the PHRR and total heat release (THR) by 39.2 % and 15.5 %, respectively. The improved fire retardancy of epoxy nanocomposite was attributed to the coaction of zinc hydroxystannate, β-Ni(OH)$_2$ and g-C_3N_4 during combustion. Additionally, the LDH-modified montmorillonite (LM) nanosheets were reported by Wang et al. and combined with intumescent flame retardant (IFR) for ABS [26]. The obtained LM nanosheets featured better flame-retardant performances than LDH and montmorillonite due to the improved condensed-phase effect. Obviously, grafting compounds with catalytic charring effect onto the surface of 2D nanosheets contributes to enhancing their dispersion and condensed-phase effect [27–30], which is expected to increase their flame-retardant efficiency and make them meet the industrial requirements (endowing polymers with a LOI of >27.0 % and a UL-94 V-0 rating).

In this work, to enhance the condensed-phase effect of g-C_3N_4 nanoflakes, the phosphorus and cerium were grafted onto their surface to create phosphorus/cerium-doped g-C_3N_4 (Ce/P-CN). The impacts of Ce/P-CN on the thermal stability, mechanical properties, and fire retardancy of ABS were investigated in detail, and the condensed-phase mode-of-action was studied by different tests. Notably, 10 wt% Ce/P-CN increased the LOI and UL-94 classification of ABS to 28.6 % and V-0, making it superior to many previous 2D nanoadditives. The ABS/(Ce/P-CN) nanocomposites featured well-preserved thermal stability and obviously enhanced mechanical strength. Therefore, the advanced ABS/(Ce/P-CN) nanocomposites with superior overall performances show great potential in various industrial applications.

2. Experimental

2.1. Materials

ABS resin (DG-417) was bought from Tianjin Dagu Chemical Co., Ltd (China). Carbamide and cerium (III) nitrate hexahydrate (Ce (NO$_3$)$_3$·6H$_2$O) were supplied by Shanghai Aladdin Reagent Co., LTD (China). Sulphuric acid and diammonium phosphate were provided from Shanghai Chemical Reagent Co., LTD (China).

2.2. Preparation of phosphorus-doped C_3N_4 (bulk P-CN)

10 g urea and 10 mL diammonium phosphate solution (concentration: 10% w/w) were added in a 100 mL beaker. The mixture was

continuously stirred for 20–30 min to become transparent, and the obtained solution was placed at 80 °C for 48–72 h to remove water. The resultant solid product was ground into powder and calcined at high temperatures in a muffle furnace. After cooling to room temperature, the yellow powder (bulk P-CN) was obtained.

2.3. Liquid-phase exfoliation of bulk P-CN

Bulk P-CN was introduced into sulfuric acid solution (concentration: 25% w/w), and stirred for 48 h to form a light-yellow suspension. The suspension was centrifuged at 8000 r/min for 3 min, and the supernatant was decanted. The resulting pellet was re-suspensed in deionized water and centrifuged again. Such washing process was repeated several times until the supernatant became neutral. The pellet was vacuum-dried at 80 °C for 24 h, and then ground at room temperature to form powder-like product (AD P-CN).

2.4. Fabrication of Ce/P-CN nanosheets

0.1 g of ADP-CN and 200 mL of deionized water were introduced into a 250 mL beaker, and ultrasonic stirring was conducted for 30 min. Then, 5 g of Ce(NO$_3$)$_3$·6H$_2$O was added, and stirred at 60 °C for 5 h to form a white suspension. The crude product was obtained by filtration, and washed with deionized water for several times, followed by drying at 80 °C for 24 h. As-prepared light-yellow product was denoted as Ce/P-CN.

2.5. Preparation of ABS/(Ce/P-CN) nanocomposites

The fabrication procedure of ABS/(Ce/P-CN) nanocomposite is as follows. Both ABS and Ce/P-CN were dried at 80 °C for 12 h in an oven, and then they were transferred into a Thermo Hakker Rheometer for melt-blending at 200 °C and a rotor speed of 50 rpm for 12 min. Then, the obtained composite was placed in a mould, and heated at 180 °C for 6 min and hot-compressed at 12 MPa for 8 min to prepare specimens used in different tests. Based on the Ce/P-CN content (0.5, 1, 2, 5 and 10 wt%), the nanocomposite was named as ABS/(Ce/P-CN)0.5, ABS/(Ce/P-CN)1, ABS/(Ce/P-CN)2, ABS/(Ce/P-CN)5, and ABS/(Ce/P-CN)10, respectively. According to the above method, the ABS nanocomposite containing 10 wt% P-CN, 10 wt% AD P-CN or 9.5 wt% P-CN + 0.5 wt% CeO$_2$ was also prepared, and defined as ABS/P-CN10, ABS/AD P-CN10, or ABS/P-CN/CeO$_2$.

2.6. Characterization

The chemical structures of nanomaterials and residual chars were analyzed by Fourier-transform infrared (FTIR) spectroscopy (Nicolet-5700, Thermo Company, USA) using KBr pellet method. The surface chemical information was collected *via* X-ray photoelectron spectroscopy (XPS, Kratos AXIS Ultra DLD, Japan). Transmission electron microscopy (TEM) was conducted by a JEM-1230 TEM microscope (JEOL, Japan), and high-angle annular dark-field scanning transmission electron microscopy (HAADF-STEM) was conducted on a Tecnai G2 F30 S-TWIN microscope, which was coupled with an energy dispersive X-ray (EDX) spectrometer. For the TEM observation of Ce/P-CN, its specimen was prepared by dispersing it in distilled water to form the suspension, and for those of ABS/(Ce/P-CN) composites, their specimens were obtained by freezing ultrathinned sectioning with a thickness of ~80 nm. X-ray diffraction (XRD, Bruker AXS D8 Advance, Germany) was applied to investigate the chemical structures of nanoparticles and ABS nanocomposites. Scanning was conducted in the range of $2\theta=2°-40°$. The thermal stability of the powdered samples was evaluated by a thermogravimetric analyzer (TGA, Q600SDT, TA instruments, USA) at a ramp rate of 10 °C/min with a nitrogen flow. Based on ASTM D-638, tensile test was carried out on an AG-IS universal tester at a tensile rate of 100 mm/min. The dumbbell-type specimen was prepared, of which

the narrow section was 33 mm * 6 mm * 3.2 mm in size. For each sample, five replicates were taken, and the average and standard deviation were reported. The limiting oxygen index (LOI) was determined by an oxygen index apparatus (PX-01-005, Phoenix, China) according to ASTM D2863 with the specimen size of 130 mm * 6.5 mm * 3 mm. The UL-94 rating was evaluated using a horizontal-vertical burning chamber (CZF-3, Jiangning, China) based on ISO-1210, and the specimen was 130 mm * 13 mm * 3 mm in size. The cone calorimetry test was undertaken by a cone calorimeter (FTT, UK) using a heat flux of 35 kW/m^2 based on ISO 5660-1. Three replicates were used for each dose, and the average and standard deviation were reported. The micro-morphology and surface component of char obtained from cone calorimetry test were characterized by a scanning electron microscope (SEM, Hitachi S-4800 (II), Japan), which was integrated with an EDX spectrometer. The graphitization degree of char was investigated by a Raman spectrometer (DXR2xi, Thermo Scientific, USA).

3. Results and discussions

3.1. Synthesis and characterization of Ce/P-CN

The synthesis route of Ce/P-CN is shown in Fig. 1a, and its transmission electron microscopy (TEM), STEM-HAADF and energy dispersive X-ray (EDX) mapping images are presented in Figs. 1b, c and S1.
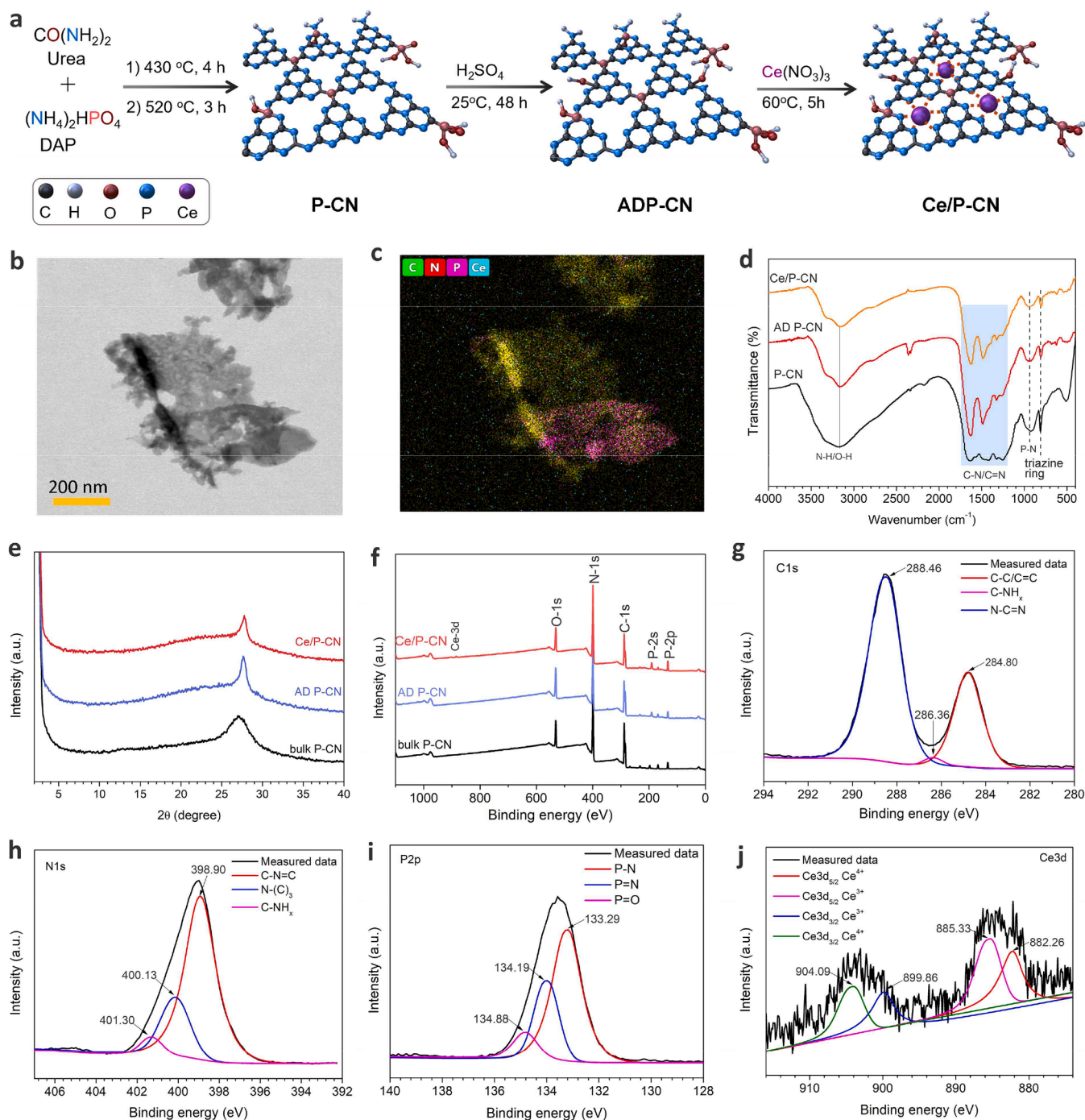
Fig. 1. (a) Preparation of Ce/P-CN nanosheets; (b) TEM and (c) C/N/P/Ce elemental mapping of Ce/P-CN; (d) FTIR, (e) XRD and (f) XPS full-scan spectra of bulk P-CN, AD P-CN and Ce/P-CN; and (g) C1s, (h) N1s, (i) P2p and (j) Ce3d high-resolution XPS spectra of Ce/P-CN.

Obviously, the TEM and STEM-HAADF micrographs of Ce/P-CN in Figs. 1b, S1a and b confirm its nanosheet structure. As presented in Figs. 1c and S1c, the C, N, P, and Ce atoms are evenly distributed on the surface of the Ce/P-CN flake. Hence, these images demonstrate that the Ce/P-doped g-C$_3$N$_4$ nanoflakes are successfully fabricated. The Fourier-transform infrared (FTIR) spectra of the P-doped g-C$_3$N$_4$ intermediates (bulk P-CN and AD P-CN) and Ce/P-CN are compared in Fig. 1d. All FTIR spectra display the typical characteristic absorption bands of C$_3$N$_4$ nanoplates at 1200–1680 and 810 cm^{-1}, belonging to C-N/C=N and tri-triazine ring, respectively. The absorption peak at 3150 cm^{-1} is assigned to the N-H/O-H groups. Notably, the peak of P-N group at 950 cm^{-1} further confirms that the phosphorus atom is successfully doped into the C$_3$N$_4$ nanosheets. In Fig. 1e, the bulk P-CN, P-CN and Ce/P-CN display similar X-ray diffraction (XRD) patterns. The characteristic peak at 27.4° is attributed to the (002) crystal plane of the nitrogen carbide nanosheets. Clearly, the Ce and P doping does not affect the crystal structure of the g-C$_3$N$_4$ nanoflakes. The X-ray photoelectron spectroscopy (XPS) results in Fig. 1c and Table S1 further indicate that both P and Ce elements exist on the surface of Ce/P-CN nanosheets. The O element can be detected in the surfaces of the bulk P-CN, AD P-CN, and Ce/P-CN because their surfaces are oxidized during fabrication [31,32]. The high-resolution C1s spectrum of Ce/P-CN in Fig. 1g can be deconvoluted

into three components, including C-C/C=C (284.80 eV), C-NH$_x$ (286.36 eV) and N-C=N (288.46 eV). There are four deconvoluted peaks at 397.90, 398.90, 400.53 and 404.92 eV in the N1s XPS spectrum of Ce/P-CN (see Fig. 1h), belonging to C-N=C, N-(C)$_3$, C-NH$_x$ and C-NH-C, respectively. The peaks at 133.29, 134.19 and 134.88 eV in the P2p XPS spectrum of Ce/P-CN are assigned to P-N, P=N, and P=O structures (see Fig. 1i). The Ce3d spectrum of Ce/P-CN (see Fig. 1j) confirms the existence of Ce^{3+} (885.33 and 899.86 eV) and Ce^{4+} (882.26 and 904.09 eV) states. All these results confirm the phosphorus/cerium-doping of Ce/P-CN.

3.2. Uniform dispersion and enhanced mechanical strength

The dispersion of nanoadditives determines the overall performances of polymer nanocomposites. The dispersion of Ce/P-CN within the ABS matrix was investigated by TEM. Under different additions (1, 5, and 10 wt%), the Ce/P-CN nanosheets can be uniformly dispersed in ABS (see Fig. 2a–c). At higher magnification, the lamellar structure of Ce/P-CN can be observed, and its size is approximately 200–500 nm (see Fig. 2a$_1$–c$_1$). The XRD patterns of ABS and ABS/(Ce/P-CN) nanocomposites are displayed in Fig. 2d. Obviously, the characteristic peak of Ce/P-CN cannot be found in the XRD patterns of ABS/(Ce/P-CN)1, ABS/
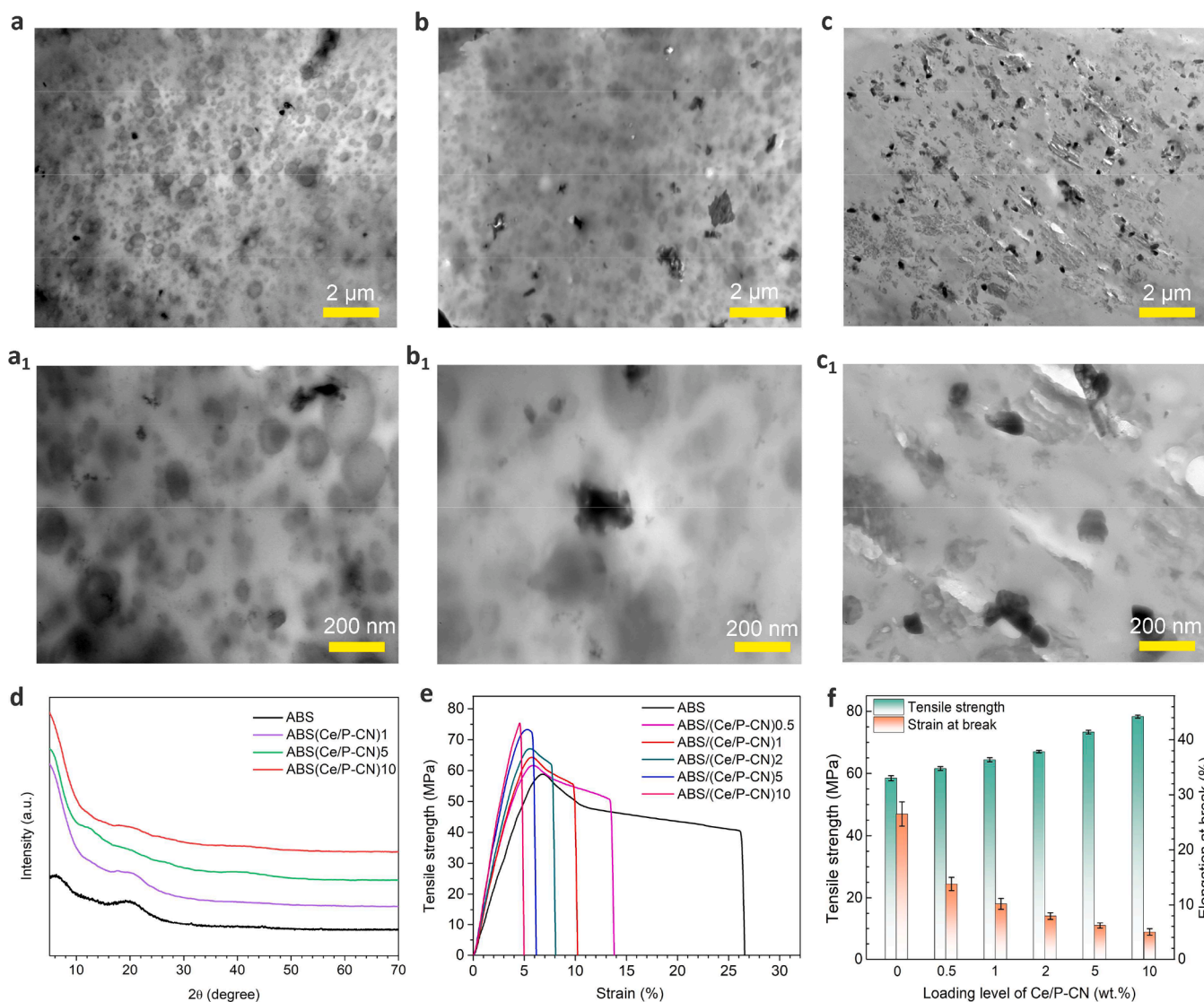
Fig. 2. TEM images of (a, a$_1$) ABS/(Ce/P-CN)1, (b, b$_1$) ABS/(Ce/P-CN)5, and (c, c$_1$) ABS/(Ce/P-CN)10 nanocomposites; and (d) XRD patterns, (e) tensile stress-strain curves, and (f) tensile parameters of ABS and ABS/(Ce/P-CN) nanocomposites.

(Ce/P-CN)5 and ABS/(Ce/P-CN)10 nanocomposites, further confirming the homogeneous dispersion of Ce/P-CN in the ABS matrix. Obviously, the evenly dispersed Ce/P-CN contributes to realizing the high performances of ABS nanocomposites.

The tensile properties of ABS and ABS nanocomposites were investigated, with the stress-strain curves shown in Figs. 2e, f and S2, and the tensile property parameters listed in Table S2. The tensile strength and elongation at break of virgin ABS are 58.5 MPa and 26.5 %, respectively (see Fig. 2e and Table S2). The tensile strength of ABS/(Ce/P-CN) nanocomposite is gradually increased with the increasing addition of Ce/P-CN (see Fig. 2f). For instance, the tensile strength of ABS/(Ce/P-CN)10 is the highest among all ABS/(Ce/P-CN) samples, which reaches up to 78.3 MPa and is 33.8 % higher than that of ABS. The enhanced mechanical robustness of ABS/(Ce/P-CN) nanocomposite is mainly due to the reinforcing effect of the well-dispersed Ce/P-CN nanoflakes. Meanwhile, the addition of Ce/P-CN reduces the elongation at break of ABS/(Ce/P-CN) nanocomposite. Notably, compared with ABS/P-CN10 and ABS/P-CN/CeO$_2$, ABS/(Ce/P-CN)10 exhibits much higher tensile strength (see Fig. S2 and Table S2), further confirming that the reinforcing effect of Ce/P-CN is better than those of P-CN and P-CN/CeO$_2$. In sum, the well-dispersed Ce/P-CN nanoflakes can effectively improve the mechanical strength of ABS due to its lamellar structure, indicative of its extensive application prospects.

3.3. Enhanced thermal stability

The thermogravimetric (TG) curves of the bulk P-CN, P-CN and Ce/P-CN are shown in Fig. 3a. The Ce-modification reduces the initial decomposition temperature (T_i, temperature at 5 % mass loss) of Ce/P-CN due to its catalyzing carbonization function. Compared with the bulk P-CN (501 °C), the T_i of Ce-P-CN is reduced to 403 °C by 19.6 %. At 800 °C, the char yield of the bulk P-CN is 43.91 wt%, while that of Ce/P-CN is increased to 52.21 wt% by 18.9 %. Obviously, the high T_i and superior char-forming ability of Ce/P-CN is expected to enhance the thermal stability of ABS.

The thermal stability of ABS and ABS/(Ce/P-CN) nanocomposites was investigated by TGA technique under nitrogen atmosphere, with the TG and derivative TG (DTG) curves shown in Fig. 3b and c. The T_i, temperature at maximum weight loss (T_{max}) and residue at 600 °C are listed in Fig. 3d and Table S3. As shown in Fig. 3b and d and Table S3, the introduction of Ce/P-CN has slight effect on the initial decomposition temperature of ABS because of its high T_i (403 °C). For instance, the T_i values of ABS/(Ce/P-CN)5 and ABS/(Ce/P-CN)10 reach 374 and 373 °C, respectively, which are very close to that of ABS (378 °C). Notably, the Ce/P-CN nanosheets effectively retards the thermal decomposition of the ABS matrix and promotes the char formation at high temperatures (see Fig. 3c and d and Table S3). All ABS/(Ce/P-CN) nanocomposites show higher T_{max} than virgin ABS. For instance, the T_{max} of ABS/(Ce/P-CN)10 is increased from 417 °C of virgin ABS to 432 °C by 15 °C. Moreover, the char residue of ABS/(Ce/P-CN)10 at 600 °C reaches 6.57 wt%, which is increased by approximately 3.5 folds relative to that of ABS. Hence, the introduction of Ce/P-CN not only effectively maintains the high initial decomposition temperature of ABS, but also significantly enhances the high-temperature stability and char-forming ability. The superior high-temperature stability and char-forming ability of ABS/(Ce/P-CN) nanocomposite confirms its fire retardancy to some extents [33–35].

3.4. Extraordinary fire retardancy

The fire retardancy of ABS, ABS/P-CN10, ABS/AD P-CN10, ABS/P-CN/CeO$_2$ and ABS/(Ce/P-CN) was investigated by cone calorimetry, LOI
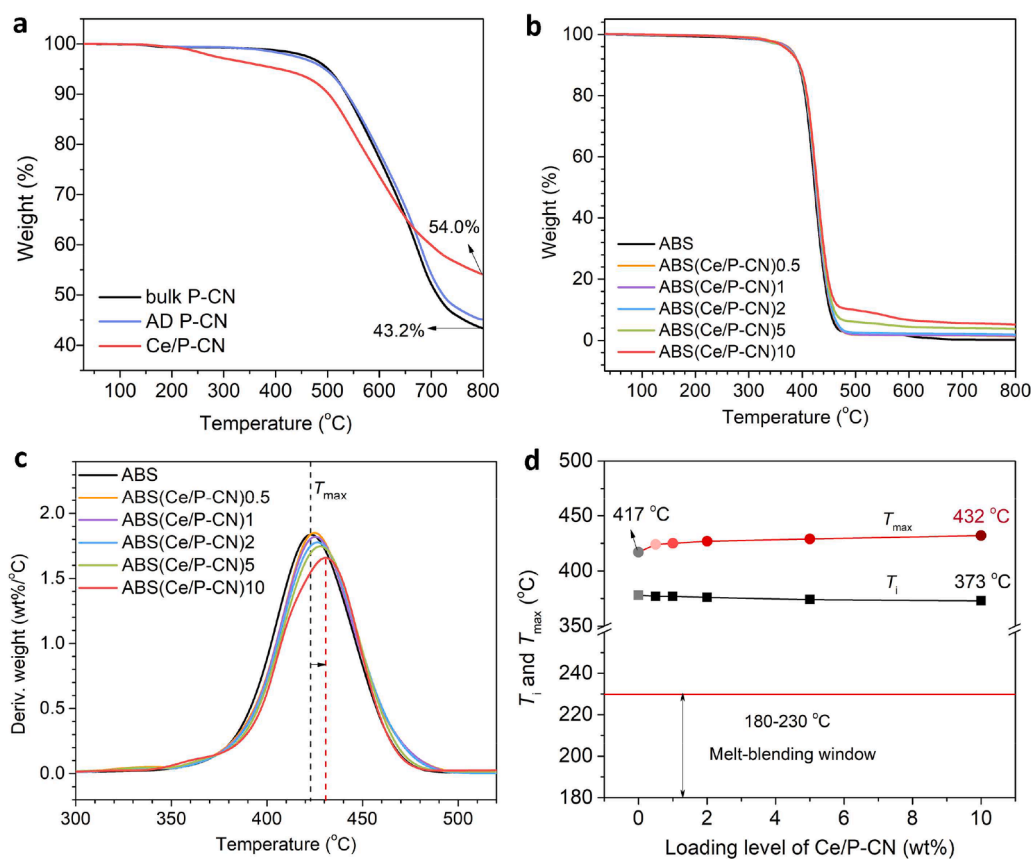
Fig. 3. (a) TG curves of bulk P-CN, AD P-CN and Ce/P-CN under nitrogen atmosphere; (b) TG, and (c) DTG curves for ABS and ABS/(Ce/P-CN) samples in N$_2$ condition; and (d) T_i and T_{max} of ABS/(Ce/P-CN) as a function of Ce/P-CN content.

and UL-94 measurements. The heat release rate and smoke production rate curves of all ABS samples obtained from cone calorimetry tests are presented in Figs. 4a, b and S3, with the combustion data listed in Table S4. Among all samples, ABS exhibits the highest peak heat release rate (PHRR) and total heat release (THR), which are up to 752 kW/m² and 105 MJ/m², respectively, indicative of its poor flame retardancy (see Fig. 4a and Table S4). Ce/P-CN effectively suppressed the heat release of the ABS matrix during combustion. In comparison to ABS, the PHRR and THR of ABS/(Ce/P-CN)10 decrease to 346 kW/m² and 89 MJ/m², by 54.0 % and 15.2 % (see Fig. 4c and Table S4), confirming the outstanding heat suppression effect of Ce/P-CN.

Moreover, both PHRR and THR of ABS/(Ce/P-CN)10 are lower than those of ABS/P-CN10, ABS/AD P-CN10, and ABS/P-CN/CeO₂ (see Fig. S3a and Table S4), confirming that the synergistic effect between Ce, P and C₃N₄ endows Ce/P-CN with better suppression effect towards

heat release of the ABS matrix. In Table S4, the average mass loss rate (AMLR) of ABS/(Ce/P-CN) nanocomposite is also gradually reduced with increasing Ce/P-CN loading level and lower than those of ABS, ABS/P-CN10, ABS/AD P-CN10, and ABS/P-CN/CeO₂, further proving its slower combustion. Additionally, the time to ignition (TTI) of ABS/(Ce/P-CN) shows an increasing trend as the Ce/P-CN addition increases. All these results indicates that the introduction of Ce/P-CN significantly enhances the fire-retardant and anti-ignition performances of ABS due to the synergistic effect between cerium, phosphorus and g-C₃N₄ nanosheets.

Besides fire retardancy and anti-ignition, the smoke suppression is another critical performance to evaluate the fire safety of materials. As shown in Fig. 4b and Table S4, ABS released a great deal of toxic smoke during combustion because of its intrinsic flammability. Thus, the peak smoke production rate (PSPR) and total smoke production (TSP) of ABS
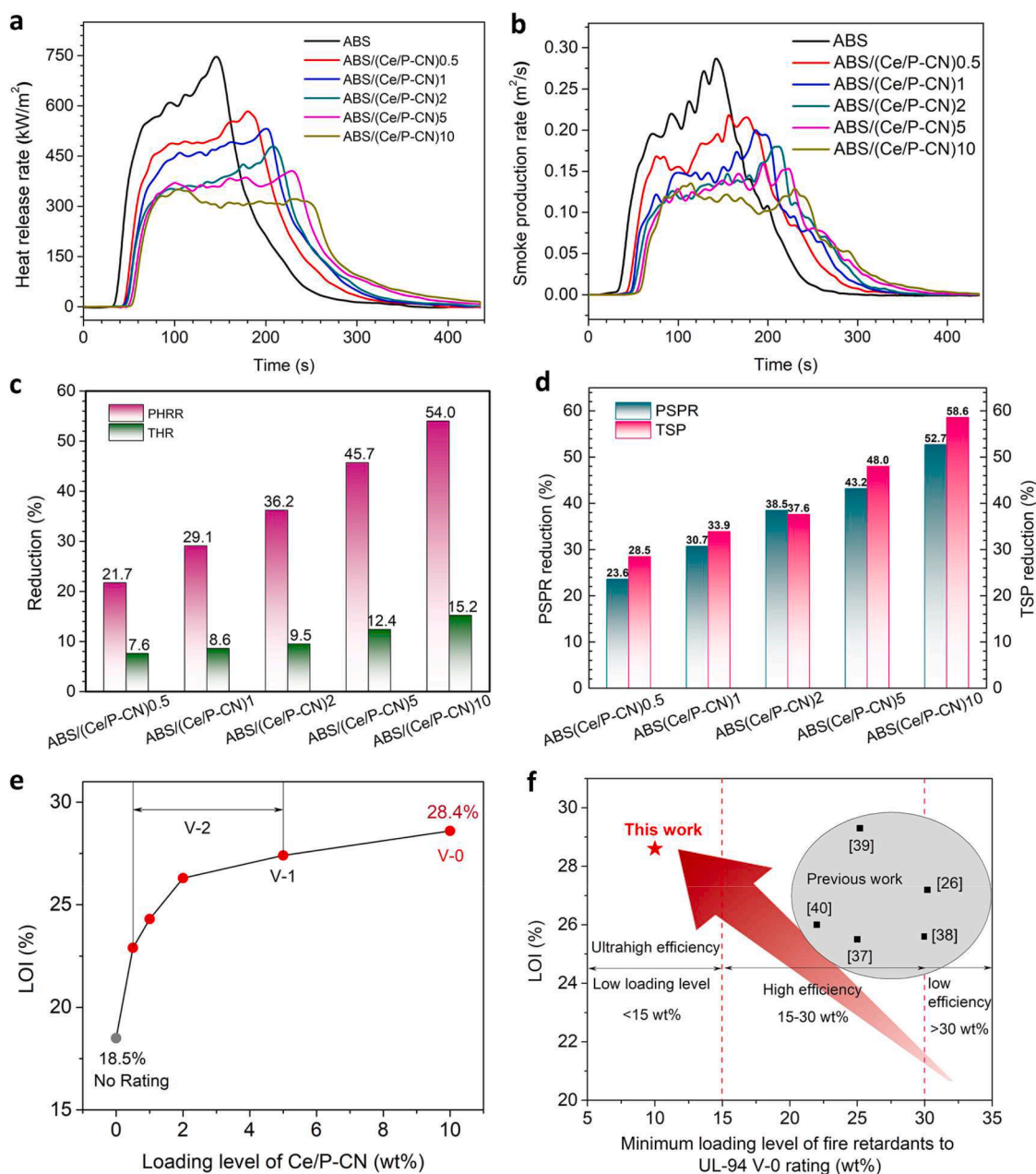
Fig. 4. (a) Heat release rate and (b) smoke production rate curves of ABS and ABS/(Ce/P-CN) samples; the reductions of ABS/(Ce/P-CN) in (c) heat release and (d) smoke production compared with ABS; (e) LOI and UL-94 rating of ABS/(Ce/P-CN) as a function of Ce/P-CN content; and (f) LOI and flame retardant addition to UL-94 V-0 rating of ABS/(Ce/P-CN)10 and previous flame-retardant ABS samples.

reach 0.296 m^2/s and 44.2 m^2, respectively. The smoke suppression of ABS/(Ce/P-CN) nanocomposites is significantly enhanced because Ce/P-CN is effective in inhibiting combustion and promoting carbonization. When the Ce/P-CN concentration increases to 10 wt%, the PSPR and TSP of ABS/(Ce/P-CN)10 are reduced to 0.140 m^2/s and 18.3 m^2, with 52.7 % and 58.6 % decreases relative to those of ABS (see Fig. 4d and Table S4). In addition, ABS/(Ce/P-CN)10 also exhibits much lower PSPR and TSP than ABS/P-CN10, ABS/AD P-CN10, and ABS/P-CN/CeO$_2$ (see Fig. S3b and Table S4). Hence, adding Ce/P-CN obviously improves the smoke suppression of ABS in addition to fire retardancy and anti-ignition. The enhanced fire safety of ABS/(Ce/P-CN) is mainly due to the barrier function of C$_3$N$_4$ nanoflakes and catalytic carbonization function of Ce and P atoms [43–46].

In industries, the LOI and UL-94 classification are the basic indexes to evaluate the flame retardancy of materials. The LOI values and UL-94 ratings of ABS and its nanocomposites are listed in Fig. 4e and Table S4. Due to the high flammability, ABS displays a low LOI value of 18.5 %, and it cannot pass any rating in UL-94 test. With the introduction of Ce/P-CN, the LOI and UL-94 rating of ABS/(Ce/P-CN) nanocomposite are significantly increased. Only 0.5 wt% of Ce/P-CN increases the UL-94 classification of ABS/(Ce/P-CN)0.5 to V-2. The ABS/(Ce/P-CN)5 nanocomposite with 5 wt% of Ce/P-CN shows a high LOI of 27.4 % and a UL-94 V-1 rating. Notably, when the Ce/P-CN content reaches 10 wt%, the LOI and UL-94 classification of ABS/(Ce/P-CN)10 increase to 28.6 % and V-0, respectively, indicating that it can be defined as a self-extinguishing material, thus meeting the industrial requirements. Moreover, ABS/(Ce/P-CN)10 shows much higher LOI value and UL-94 rating than ABS/P-CN10, ABS/AD P-CN10, and ABS/P-CN/CeO$_2$, indicative of its higher flame-retardant efficiency due to the synergistic effect between g-C$_3$N$_4$, phosphorus and cerium. The LOI and flame retardant addition to UL-94 V-0 rating of ABS/(Ce/P-CN)10 and previous flame-retardant ABS samples are compared in Fig. 4f, and their comprehensive property data are listed in Table 1 [1,15,26,31,36–42]. Obviously, ABS/(Ce/P-CN)10 shows the lowest flame-retardant addition among all ABS samples with a UL-94 V-0 rating, demonstrating the highest flame-retardant efficiency of Ce/P-CN among all reported flame retardants for ABS. Meanwhile, ABS/(Ce/P-CN)10 displays high LOI (28.6 %) and tensile strength enhancement (33.8 %), making it superior to previous flame-retardant ABS counterparts. In sum, Ce/P-CN features high flame-retardant efficiency and multifunctionality, enabling ABS to achieve superior flame retardancy and mechanical robustness.

3.5. Prominent condensed-phase effect

As mentioned above, the superior fire safety of ABS/(Ce/P-CN) nanocomposites is mainly due to the condensed-phase effect of Ce/P-CN. To analyze the condensed-phase effect of Ce/P-CN, the char residues of ABS and ABS/(Ce/P-CN) obtained from cone calorimetry tests were studied by digital camera, SEM, EDX, FTIR and Raman spectrometry, with the results shown in Figs. 5 and S4 and Table S5. As presented in Fig. 5a, ABS only left very small amounts of broken and fragile chars after test, further indicating its poor char-forming ability. With the introduction of Ce/P-CN, the char structure becomes compact and continuous (see Figs. 5b and c and S4). The formation of such dense chars contributes to suppressing the heat release and smoke generation during combustion [47–49]. It is also noteworthy that the nitrogen, phosphorus, and cerium contents of ABS char are gradually increased with increasing Ce/P-CN addition (see Fig. 5d and Table S5). Such results further confirm that the g-C$_3$N$_4$ nanosheets, and phosphorus and cerium atoms in Ce/P-CN all function in the condensed phase during combustion, thus enhancing the fire safety of ABS nanocomposite.

Moreover, the FTIR spectra of ABS, ABS/(Ce/P-CN)1, ABS/(Ce/P-CN)5, and ABS/(Ce/P-CN)10 chars are presented in Fig. 5e. The absorption peaks of O-H/N-H, C=C, C-O-C, and C-C bonds can be found at 3460, 1610, 1260 and 1010 cm^{-1} in all FTIR spectra. In addition to the above peaks, the characteristic peaks of P-N and P-O-C structures appear at 1400 and 1110 cm^{-1} in the FTIR spectra of ABS/(Ce/P-CN)1, ABS/(Ce/P-CN)5, and ABS/(Ce/P-CN)10 chars, further confirming that both g-C$_3$N$_4$ nanosheets and phosphorus atom in Ce/P-CN function in the condensed phase to promote the formation of compact and dense char layers in the burning process [50,51]. The degrees of graphitization of ABS and ABS/(Ce/P-CN) chars can be compared quantitatively by calculating their integral area ratio (I_D/I_G) values of D band to G band in Raman spectra (see Fig. 5e). The I_D/I_G values of ABS samples follow the sequence: ABS (2.70) > ABS/(Ce/P-CN)1 (2.56) > ABS/(Ce/P-CN)1 (2.47) > ABS/(Ce/P-CN)10 (2.32). Obviously, the introduction of Ce/P-CN increases the graphitization degree of ABS char, which is conducive to inhibiting the heat release and smoke generation during combustion [52,53]. In sum, the C$_3$N$_4$ nanosheets and P and Ce atoms in Ce/P-CN all promote the formation of a dense and continuous char layer on the matrix surface, which restrains the heat exchange and smoke generation, thus endowing ABS with superior fire safety.

4. Conclusion

In this work, the cerium/phosphorus-modified C$_3$N$_4$ (Ce/P-CN) nanosheets were fabricated and applied in the preparation of advanced fire-safe ABS nanocomposites. The Ce/P-CN nanoflakes can be homogeneously dispersed within the ABS matrix, thus obviously increasing the tensile strength of ABS nanocomposite by their reinforcing effect. In detail, adding 10 wt% of Ce/P-CN increases the tensile strength by 33.8 %. Meanwhile, the introduction of Ce/P-CN effectively maintains the high initial degradation temperature of ABS and endows it with superior high-temperature stability and char-formation property. Due to the barrier effect of C$_3$N$_4$ nanosheets and catalytic carbonization effect of phosphorus and cerium, the ABS/(Ce/P-CN) nanocomposites show outstanding anti-ignition, fire retardancy and smoke suppression. Notably, 10 wt% of Ce/P-CN can increase the LOI and UL-94 rating of ABS/(Ce/P-CN)10 to 28.6 % and V-0, respectively, demonstrating the high flame-retardant efficiency of Ce/P-CN towards ABS. Therefore, this

Table 1
Property comparison of ABS/(Ce/P-CN)10 and previous flame-retardant ABS samples.

Refs.	FR addition (wt%)	LOI (%)	UL-94 rating	Reduction in PHRR (%)	Variation in tensile strength (%)
[36]	5	27.9	V-1	45.0 %	+31.0 %
[1]	1	26.1	V-2	51.0 %	+29.0 %
[31]	2	26.1	V-2	32.4 %	+24.3 %
[37]	25	25.5	V-0	49.6 %	+0.5 %
[38]	30	25.6	V-0	/	−32.0 %
[39]	25	29.3	V-0	53.5 %	−17.8 %
[40]	22	26.0	V-0	77.1 %	+6.1 %
[26]	30	27.2	V-0	63.3 %	−16.0 %
[41]	25	26.5	V-0	64.6 %	+4.2 %
[15]	2	23.5	/	23.3 %	+22.7 %
[42]	2	21.5	/	17.5 %	+4.8 %
This work	**10**	**28.6**	**V-0**	**54.0 %**	**+33.8 %**
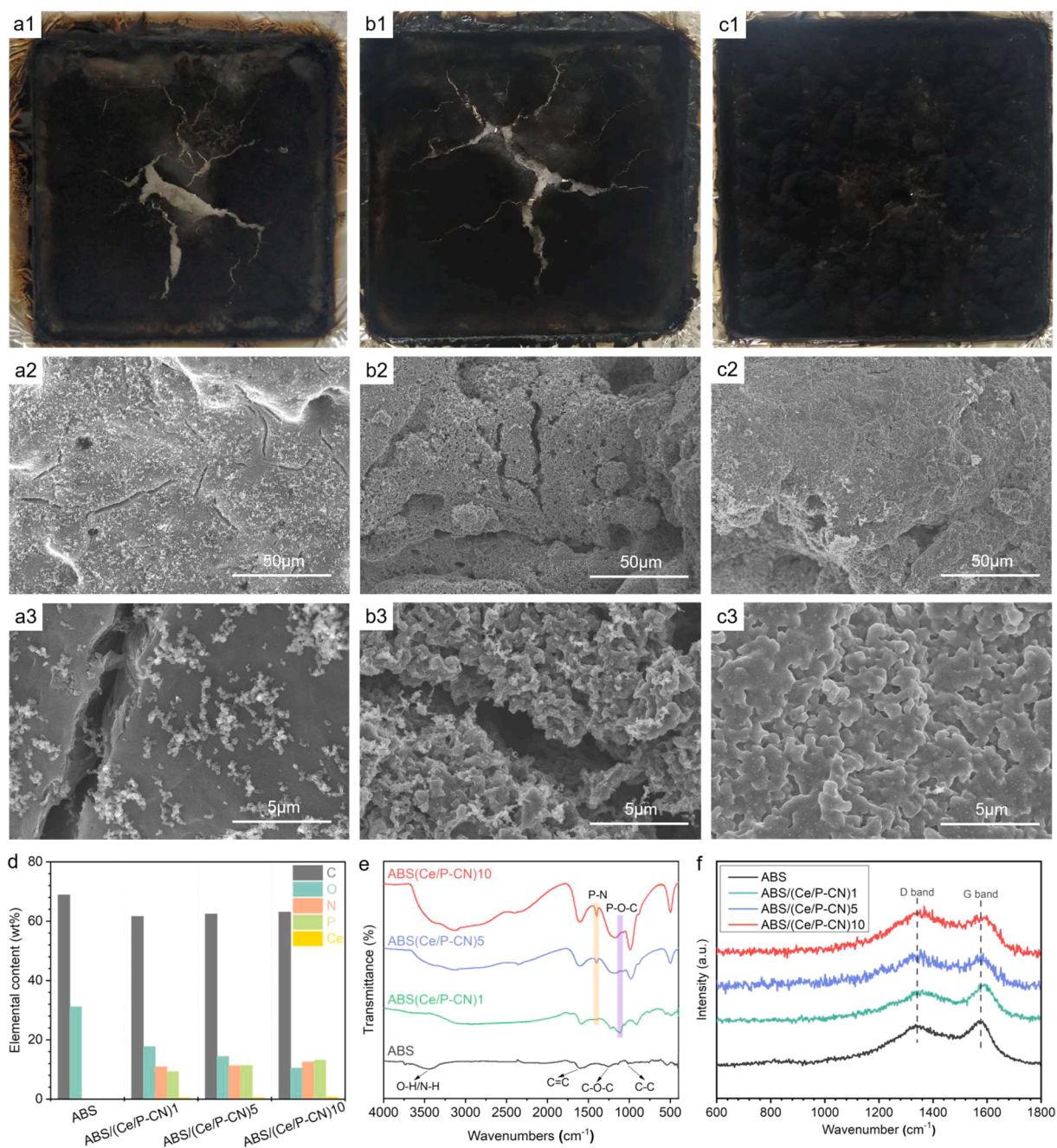
Fig. 5. Digital and SEM photos of (a1–a3) ABS, (b1–b3) ABS/(Ce/P-CN)1, and (c1–c3) ABS/(Ce/P-CN)10 residues after cone calorimetry; (d) element contents of ABS, ABS/(Ce/P-CN)1, ABS/(Ce/P-CN)5, and ABS/(Ce/P-CN)10 chars obtained from EDX; and (e) FTIR, and (f) Raman spectra of ABS, ABS/(Ce/P-CN)1, ABS/(Ce/P-CN)5, and ABS/(Ce/P-CN)10 chars.

work creates a multifunctional nanoadditive to simultaneously enhance the mechanical strength and fire safety of ABS without compromising the thermal stability, thus extending its industrial applications.

CRediT authorship contribution statement

Guobo Huang: Writing – original draft, Funding acquisition, Formal analysis, Data curation, Conceptualization. **Siqi Huo:** Writing – review & editing, Formal analysis. **Jiahao Ren:** Methodology, Investigation. **Wei Chen:** Methodology, Formal analysis. **Haiqin Yang:** Methodology, Investigation. **Shenwei Xiao:** Methodology, Investigation, Formal analysis. **Tianle Wang:** Writing – original draft, Methodology, Investigation. **Hong Peng:** Writing – review & editing, Formal analysis. **Pingan Song:** Writing – review & editing, Supervision, Formal analysis.

Declaration of competing interest

Data availability

No data was used for the research described in the article.

Acknowledgments

Supplementary materials

Supplementary material associated with this article can be found, in the online version, at doi:10.1016/j.apmt.2024.102191.

References

[1] G. Huang, W. Chen, T. Wu, H. Guo, C. Fu, Y. Xue, K. Wang, P. Song, Multifunctional graphene-based nano-additives toward high-performance polymer nanocomposites with enhanced mechanical, thermal, flame retardancy and smoke suppressive properties, Chem. Eng. J. 410 (2021) 127590.

[2] S. Olivera, H.B. Muralidhara, K. Venkatesh, K. Gopalakrishna, C.S. Vivek, Plating on acrylonitrile–butadiene–styrene (ABS) plastic: a review, J. Mater. Sci. 51 (2016) 3657–3674.

[3] G. Huang, D. Han, Y. Jin, P. Song, Q. Yan, C. Gao, Fabrication of nitrogen-doped graphene decorated with organophosphor and lanthanum toward high-performance ABS nanocomposites, ACS Appl. Nano Mater. 1 (2018) 3204–3213.

[4] R.K. Jian, L. Chen, S.Y. Chen, J.W. Long, Y.Z. Wang, A novel flame-retardant acrylonitrile-butadiene-styrene system based on aluminum isobutylphosphinate and red phosphorus: flame retardance, thermal degradation and pyrolysis behavior, Polym. Degrad. Stab. 109 (2014) 184–193.

[5] Q. Wu, F. Ran, L. Dai, C. Li, R. Li, C. Si, A functional lignin-based nanofiller for flame-retardant blend, Int. J. Biol. Macromol. 190 (2021) 390–395.

[6] B. Perret, K. Pawlowski, B. Schartel, Fire retardancy mechanisms of arylphosphates in polycarbonate (PC) and PC/acrylonitrile-butadiene-styrene: the key role of decomposition temperature, J. Therm. Anal. Calorim. 97 (2009) 949–958.

[7] N.F. Attia, E.S. Goda, M. Nour, M. Sabaa, M. Hassan, Novel synthesis of magnesium hydroxide nanoparticles modified with organic phosphate and their effect on the flammability of acrylonitrile-butadiene styrene nanocomposites, Mater. Chem. Phys. 168 (2015) 147–158.

[8] P. Song, Z. Cao, S. Fu, Z. Fang, Q. Wu, J. Ye, Thermal degradation and flame retardancy properties of ABS/lignin: effects of lignin content and reactive compatibilization, Thermochim. Acta 518 (2011) 59–65.

[9] A.B. Morgan, J.L. Jurs, J.M. Tour, Synthesis, flame-retardancy testing, and preliminary mechanism studies of nonhalogenated aromatic boronic acids: a new class of condensed-phase polymer flame-retardant additives for acrylonitrile–butadiene–styrene and polycarbonate, J. Appl. Polym. Sci. 76 (2000) 1257–1268.

[10] B. Prieur, M. Meub, M. Wittemann, R. Klein, S. Bellayer, G. Fontaine, S. Bourbigot, Phosphorylation of lignin to flame retard acrylonitrile butadiene styrene (ABS), Polym. Degrad. Stab. 127 (2016) 32–43.

[11] S. Wang, Y. Hu, R. Zong, Y. Tang, Z. Chen, W. Fan, Preparation and characterization of flame retardant ABS/montmorillonite nanocomposite, Appl. Clay Sci. 25 (2004) 49–55.

[12] X. Wang, E.N. Kalali, J.T. Wan, D.Y. Wang, Carbon-family materials for flame retardant polymeric materials, Prog. Polym. Sci. 69 (2017) 22–46.

[13] Y. Yu, Y. Zhang, L. Xi, Z. Zhao, S. Huo, G. Huang, Z. Fang, P. Song, Interface nanoengineering of a core-shell structured biobased fire retardant for fire-retarding polylactide with enhanced toughness and UV protection, J. Clean. Prod. 336 (2022) 130372.

[14] N. Hong, J. Zhan, X. Wang, A.A. Stec, T.R. Hull, H. Ge, W. Xing, L. Song, Y. Hu, Enhanced mechanical, thermal and flame retardant properties by combining graphene nanosheets and metal hydroxide nanorods for Acrylonitrile–Butadiene–Styrene copolymer composite, Compos. Part A Appl. Sci. Manuf. 64 (2014) 203–210.

[15] S.E. Zhu, F.D. Wang, J.J. Liu, L.L. Wang, C. Wang, A.C.Y. Yuen, T.B.Y. Chen, I. I. Kabir, G.H. Yeoh, H.D. Lu, BODIPY coated on MXene nanosheets for improving mechanical and fire safety properties of ABS resin, Compos. Part B Eng. 223 (2021) 109130.

[16] H. He, P. Song, B. Yu, Z. Fang, H. Wang, Flame retardant polymeric nanocomposites through the combination of nanomaterials and conventional flame retardants, Prog. Mater. Sci. 114 (2020) 100687.

[17] Q. Chen, L. Liu, A. Zhang, W. Wang, Z. Wang, J. Zhang, J. Feng, S. Huo, X. Zeng, P. Song, An iron phenylphosphinate@ graphene oxide nanohybrid enabled flame-retardant, mechanically reinforced, and thermally conductive epoxy nanocomposites, Chem. Eng. J. 454 (2023) 140424.

[18] B.W. Liu, H.B. Zhao, Y.Z. Wang, Advanced flame-retardant methods for polymeric materials, Adv. Mater. 34 (2022) 2107905.

[19] X. Wang, W. Guo, W. Cai, J. Wang, L. Song, Y. Hu, Recent advances in construction of hybrid nano-structures for flame retardant polymers application, Appl. Mater. Today 20 (2020) 100762.

[20] H.Y. Chen, Z.Y. Chen, M. Mao, Y.Y. Wu, F. Yang, L.X. Gong, L. Zhao, C.F. Cao, P. Song, J.F. Gao, G.D. Zhang, Y.Q. Shi, K. Cao, L.C. Tang, Self-Adhesive polydimethylsiloxane foam materials decorated with MXene/Cellulose nanofiber interconnected network for versatile functionalities, Adv. Funct. Mater. 33 (2023) 2304927.

[21] Y. Shi, B. Yu, L. Duan, Z. Gui, B. Wang, Y. Hu, R.K. Yuen, Graphitic carbon nitride/phosphorus-rich aluminum phosphinates hybrids as smoke suppressants and flame retardants for polystyrene, J. Hazard. Mater. 332 (2017) 87–96.

[22] Y. Shi, C. Liu, L. Fu, F. Yang, Y. Lv, B. Yu, Hierarchical assembly of polystyrene/graphitic carbon nitride/reduced graphene oxide nanocomposites toward high fire safety, Compos. Part B Eng. 179 (2019) 107541.

[23] Y. Shi, L. Wang, L. Fu, C. Liu, B. Yu, F. Yang, Y. Hu, Sodium alginate-templated synthesis of g-C3N4/carbon spheres/Cu ternary nanohybrids for fire safety application, J. Colloid Interface Sci. 539 (2019) 1–10.

[24] H. Ma, P. Song, Z. Fang, Flame retarded polymer nanocomposites: development, trend and future perspective, Sci. China Chem. 54 (2011) 302–313.

[25] W. Xu, R. Chen, J. Xu, D. Zhong, Z. Cheng, Nickel hydroxide and zinc hydroxystannate dual modified graphite carbon nitride for the flame retardancy and smoke suppression of epoxy resin, Polym. Degrad. Stab. 182 (2020) 109366.

[26] B. Wang, B. Wu, G. Zhang, B. Yang, In-situ growth of layered double hydroxide on montmorillonite nanosheets to improve the flame retardant performance of ABS resin, J. Vinyl Addit. Technol. 29 (2023) 435–447.

[27] L.Y. Lv, C.F. Cao, Y.X. Qu, G.D. Zhang, L. Zhao, K. Cao, P. Song, L.C. Tang, Smart fire-warning materials and sensors: design principle, performances, and applications, Mater. Sci. Eng. R 150 (2022) 100690.

[28] K. Malkappa, S.S. Ray, N. Kumar, Enhanced thermo-mechanical stiffness, thermal stability, and fire retardant performance of surface-modified 2D MoS2 nanosheet-reinforced polyurethane composites, Macromol. Mater. Eng. 304 (2019) 1800562.

[29] Y. Shi, L. Fu, X. Chen, J. Guo, F. Yang, J. Wang, Y. Zheng, Y. Hu, Hypophosphite/graphitic carbon nitride hybrids: preparation and flame-retardant application in thermoplastic polyurethane, Nanomaterials 7 (2017) 259.

[30] Y. Shi, B. Yu, R.K. Zhou, Z. Gui, Y. Hu, S. Jiang, Novel CuCo2O4/graphitic carbon nitride nanohybrids: highly effective catalysts for reducing CO generation and fire hazards of thermoplastic polyurethane nanocomposites, J. Hazard. Mater. 293 (2015) 87–96.

[31] J. Ren, S. Huo, G. Huang, T. Wang, J. Feng, W. Chen, S. Xiao, P. Song, A novel P/Ni-doped g-C3N4 nanosheets for improving mechanical, thermal and flame-retardant properties of acrylonitrile–butadienestyrene resin, Chem. Eng. J. 452 (2023) 139196.

[32] M. Rong, Z. Cai, L. Xie, C. Lin, X. Song, F. Luo, Y. Wang, X. Chen, Study on the ultrahigh quantum yield of fluorescent P, O-g-C3N4 nanodots and its application in cell imaging, Chem. Eur. J. 22 (2016) 9387–9395.

[33] X. Wen, J. Min, H. Tan, D. Gao, X. Chen, K. Szymańska, B. Zielińska, E. Mijowska, T. Tang, Reactive construction of catalytic carbonization system in PP/C60/Ni (OH)2 nanocomposites for simultaneously improving thermal stability, flame retardancy and mechanical properties, Compos. Part A Appl. Sci. Manuf. 129 (2020) 105722.

[34] Z.H. Wang, A.N. Zhang, B.W. Liu, X.L. Wang, H.B. Zhao, Y.Z. Wang, Durable flame-retardant cotton fabrics with tannic acid complexed by various metal ions, Polym. Degrad. Stab. 201 (2022) 109997.

[35] W. Zhao, C.K. Kundu, Z. Li, X. Li, Z. Zhang, Flame retardant treatments for polypropylene: strategies and recent advances, Compos. Part A Appl. Sci. Manuf. 145 (2021) 106382.

[36] G. Huang, S. Huo, X. Xu, W. Chen, Y. Jin, R. Li, P. Song, H. Wang, Realizing simultaneous improvements in mechanical strength, flame retardancy and smoke suppression of ABS nanocomposites from multifunctional graphene, Compos. Part B Eng. 177 (2019) 107377.

[37] N. Wu, X. Xiu, Surface microencapsulation modification of aluminum hypophosphite and improved flame retardancy and mechanical properties of flame-retardant acrylonitrile–butadiene–styrene composites, RSC Adv. 5 (2015) 49143–49152.

[38] X. Cao, Y. Yang, H. Luo, X. Cai, High efficiency intumescent flame retardancy between Hexakis (4-nitrophenoxy) cyclotriphosphazene and ammonium polyphosphate on ABS, Polym. Degrad. Stab. 143 (2017) 259–265.

[39] W. Liu, H. Wang, L. Zou, S. Cai, X. Liu, J. Liu, X. Xie, Synergistic effect of zeolite on the nitrogen-containing phosphinate salt-based acrylonitrile–butadiene–styrene flame-retardant composite, J. Polym. Res. 29 (2022) 6.

[40] N. Wu, Z. Xiu, J. Du, Preparation of microencapsulated aluminum hypophosphite and flame retardancy and mechanical properties of flame-retardant ABS composites, J. Appl. Polym. Sci. 134 (2017) 45008.

[41] L. Xiong, S. Huang, R. Zhong, W. Tang, C. Liu, Y. Jin, Preparation, Characterization, and Performance of Lignin-based Microencapsulated Red Phosphorus Flame Retardant for ABS, J. Wuhan Univ. Technol. 37 (2022) 292–299.

[42] W. Pan, Q. Zhou, W. Yang, S. Nie, L. Xu, C. Wei, H. Lu, W. Yang, A.C.Y. Yuen, MXene-wrapped zinc hydroxystannate nanocubes toward reducing the heat, smoke and toxicity hazards of ABS resin, J. Therm. Anal. Calorim. 148 (2023) 12467–12479.

[43] J. Tao, F. Yang, T. Wu, J. Shi, H.B. Zhao, W. Rao, Thermal insulation, flame retardancy, smoke suppression, and reinforcement of rigid polyurethane foam enabled by incorporating a P/Cu-hybrid silica aerogel, Chem. Eng. J. 461 (2023) 142061.

[44] B. Xu, S. Wei, Y. Liu, M. Wu, Effects of different metal ions in phosphonitrile-modified organometallic complexes on flame retardancy of epoxy resin, Polym. Degrad. Stab. 214 (2023) 110407.

[45] T. Sai, S. Ran, S. Huo, Z. Guo, P. Song, Z. Fang, Sulfonated block ionomers enable transparent, fire-resistant, tough yet strong polycarbonate, Chem. Eng. J. 433 (2022) 133264.

[46] B. Xu, M. Wu, Y. Liu, S. Wei, Study on flame retardancy behavior of epoxy resin with phosphaphenanthrene triazine compound and organic zinc complexes based on phosphonitrile, Molecules 28 (2023) 3069.

[47] J. Liu, Z. He, G. Wu, X. Zhang, C. Zhao, C. Lei, Synthesis of a novel nonflammable eugenol-based phosphazene epoxy resin with unique burned intumescent char, Chem. Eng. J. 390 (2020) 124620.

[48] A. Zhang, J. Zhang, L. Liu, J. Dai, X. Lu, S. Huo, M. Hong, X. Liu, M. Lynch, X. Zeng, P. Burey, P. Song, Engineering phosphorus-containing lignin for epoxy biocomposites with enhanced thermal stability, fire retardancy and mechanical properties, J. Mater. Sci. Technol. 167 (2023) 82–93.

[49] B. Xu, S. Wei, Y. Liu, S. Zhao, L. Qian, Preparation of an organometallic complex based on phosphonitrile and its flame retardant application in epoxy resin, J. Mater. Res. Technol. 21 (2022) 4921–4939.

[50] W. Huang, W. He, L. Long, W. Yan, M. He, S. Qin, J. Yu, Highly efficient flame-retardant glass-fiber-reinforced polyamide 6T system based on a novel DOPO-

based derivative: flame retardancy, thermal decomposition, and pyrolysis behavior, Polym. Degrad. Stab. 148 (2018) 26–41.

[51] X. Hu, B. Wang, Z. Guo, Z. Fang, P. Chen, J. Li, Roles of phosphoramide derivatives in flame retardancy, thermal degradation and crystallization behaviors of polylactic acid, Int. J. Biol. Macromol. 219 (2022) 558–570.

[52] Q. Yang, J. Wang, X. Chen, S. Yang, S. Huo, Q. Chen, P. Guo, X. Wang, F. Liu, W. Chen, P. Song, H. Wang, A phosphorus-containing tertiary amine hardener enabled flame retardant, heat resistant and mechanically strong yet tough epoxy resins, Chem. Eng. J. 468 (2023) 143811.

[53] X. Jin, S. Cui, S. Sun, X. Gu, H. Li, X. Liu, W. Tang, J. Sun, S. Bourbigot, S. Zhang, The preparation of a bio-polyelectrolytes based core-shell structure and its application in flame retardant polylactic acid composites, Compos. Part A Appl. Sci. Manuf. 124 (2019) 105485.